Available online at www.sciencedirect.com
ScienceDirect
Nuclear Instruments and Methods in Physics Research A 565 (2006) 589–598
NUCLEAR INSTRUMENTS & METHODS IN PHYSICS RESEARCH Section A
www.elsevier.com/locate/nima

A radioactive point-source lattice for calibrating and monitoring the liquid xenon calorimeter of the MEG experiment

A. Baldini[a], C. Bemporad[a], F. Cei[a,*], S. Dussoni[b], F. Gatti[b], M. Grassi[a], T. Haruyama[c], Y. Hisamatsu[d], T. Iwamoto[d], S. Mihara[d], T. Mori[d], D. Nicolò[a], H. Nishiguchi[d], W. Ootani[d], A. Papa[a], R. Pazzi[a], R. Sawada[d], F. Sergiampietri[a], G. Signorelli[a], R. Valle[b], S. Yamada[d]

[a]*INFN and University of Pisa, Pisa, Italy*
[b]*INFN and University of Genova, Genova, Italy*
[c]*KEK, Tsukuba, Japan*
[d]*University of Tokyo, Tokyo, Japan*

Received 5 April 2006; accepted 12 June 2006
Available online 14 July 2006

Abstract

Liquid scintillator calorimeters and in particular liquid cryogenic noble gas detectors can be calibrated and monitored by the use of multiple α-sources distributed in the detector sensitive volume. For the MEG experiment we developed a method based on the use of ^{210}Po and ^{241}Am point sources deposited on thin (100 μm diameter) gold-plated tungsten wires permanently suspended in the volume and fixed at the surfaces of the large vessel containing the LXe. The method is valuable in measuring the relative QEs of all PMTs surrounding the sensitive LXe volume, in determining the LXe optical properties for the UV scintillation light and in checking the stability of the calorimeter properties during the experiment.

PACS: 06.60.Mr; 29.40.Mc; 29.40.Vj

Keywords: Calibration; Monitoring; Liquid xenon calorimeter; Radioactive sources; MEG experiment

1. Introduction

The MEG experiment, now in an advanced stage of preparation at the Paul Scherrer Institut [1], aims at detecting the process $\mu^+ \to e^+\gamma$. The present experimental upper bound for the branching ratio in the $e^+\gamma$ channel is 1.2×10^{-11} at the 90% C.L. [2]. The MEG experiment is expected to improve by 2 orders of magnitude on this limit and to be sensitive to several theoretical predictions [3].

A liquid xenon (LXe) scintillation photon detector is an essential part of the experiment and is presently under construction. It was designed to achieve superior performances such as $\Delta E_\gamma/E_\gamma = 4\%$ for the γ energy, $\Delta x_\gamma \approx 5$ mm for the position resolution, $\Delta t_\gamma \approx 120$ ps (at $E_\gamma = 52.8$ MeV; Δ stands for FWHM). The LXe calorimeter will only collect scintillation light, without any independent ionization measurement. The final detector will have an active volume of 800 l LXe and ≈ 830 PMTs. Since no such large size LXe detector was ever produced, a smaller prototype (Calorimeter Prototype) was built to gain a know-how in LXe calorimetry [4]. The prototype has an active volume of 68.6 l of LXe and was an important milestone in view of the final detector, since it gave us a practical knowledge of the behaviour of such a device.

Above all, the purification of LXe and the long-term stability are essential for ensuring an optimized light yield and performance of the detector.

The LXe calorimeter has a great intrinsic accuracy and must maintain this quality and its energy stability during

*Corresponding author. Dipartimento di Fisica dell' Università di Pisa, Largo B. Pontecorvo, 3-56127 Pisa, Italy. Tel.: +39 050 2214409; fax: +39 050 2214317.
E-mail address: fabrizio.cei@pi.infn.it (F. Cei).

0168-9002/$ - see front matter © 2006 Elsevier B.V. All rights reserved.
doi:10.1016/j.nima.2006.06.055

an experiment which uses the highest intensity stopping muon-beam ($\approx 10^8\,\mu^+\,s^{-1}$) presently available. It is therefore of the utmost importance to develop ways of setting-up and of permanently checking the calorimeter behaviour.

The MEG calorimeter is basically a large LXe volume limited by a UV-light sensitive surface. The photomultipliers ($\approx 35\%$ surface coverage) are directly immersed in the cryogenic liquid. The calorimeter physical response depends therefore on the quantum efficiency and amplification of each PMT at low temperatures and on the LXe optical properties in the UV, i.e., the Rayleigh scattering length, the refractive index and the LXe absorption length (intrinsic or possibly dependent on Xe contaminants). It is worth recalling that all PMTs must operate in the rather high fringing field of the MEG experiment superconducting COBRA solenoid ($\approx 50\,G$).

During the MEG experiment several redundant and complementary methods will be used to calibrate and monitor the calorimeter behaviour [5]. We want to discuss in detail one of these methods, peculiar to liquid detectors, which was expressly developed for our LXe calorimeter and tested in the Calorimeter Prototype. The method is based on a set of thin wires on which several point-like ^{210}Po or ^{241}Am α-sources (individual activity $\approx 300\,Bq$) are deposited (from now on: wire with point-sources $\rightarrow$ WPS); the wires are then mounted in the LXe sensitive volume. The WPS turned out to be a most effective device for determining the relative PMT QEs in the normal MEG operating conditions and to measure and check the LXe optical properties.

2. The production of the radioactive point-sources on wire and their test in cryogenic liquids

The first WPS, used for measurements in the Calorimeter Prototype, were produced by the collaboration and gave the results presented in this article. The radioactive material was ^{210}Po electrodeposited on (50 μm diameter) gold-plated tungsten wires. The ^{210}Po-lifetime ($t_{1/2} = 138\,d$) was adequate for a short test. The final WPS for the experiment must instead have a stable intensity for several years after their installation in the MEG calorimeter. The best possible radioisotope is ^{241}Am ($t_{1/2} = 430\,yr$). Unfortunately the preparation of stable and safe ^{241}Am sources requires a complicate procedure. We tried to explore the possibility of having them built by one of the several leading radioisotope companies. This search produced a voluminous correspondence, but no real result. We did not succeed in convincing one of those companies to embark in the R&D necessary for the production of the WPS, according to our specifications. Finally, we were lucky enough to find one small company (SORAD Ltd. in the Czech Republic) [6], a firm specialized in the production of ^{241}Am α-sources for smoke detectors, which accepted to perform a period of R&D and an attempt to produce the sources we needed.[1] After several months, we obtained some sample ^{241}Am WPS which are presently used in the Calorimeter Prototype. The characteristics of the normal ^{241}Am foil sources produced by SORAD and a simple description of their preparation can be found at http://www.raz-dva.cz/sorad/. The WPS produced for us are prepared by fixing small portions of the foil to a gold-plated tungsten wire by a thermocompression method.

Since pure Xenon is quite an expensive material, one has to be really sure that both the ^{210}Po and the ^{241}Am α-sources can mechanically stand cryogenic temperatures and that there is no leakage of the radioactive isotope into the LXe. We decided therefore to ask the Italian national lab. ENEA-Casaccia to perform sensitive tests on this subject. It is worth noting that commercial α-sources, because of international regulations, are tested at $-40\,^{\circ}C$ as the lowest temperature. There is no guarantee that commercial sources can be safely used at cryogenic temperatures. The normal tests which are performed at production (in the case of SORAD, by the Česky' Metrologicky' Institut), correspond to the Standards ISO 2919/1980(E), ISO 9978/1992, IAEA Safety Series no. 6/1985 (1990), BS 5288/1976, DIN 25426-Tiel 1/1988, Tiel 3/1991. The additional tests, which were performed at ENEA-Casaccia, were applied sequentially on each source in a period of several months:

(1) *Immersion test in acetone*: The source is immersed in an acetone bath at $20\,^{\circ}C$ for 6 h; the removed activity is measured.

(2) *Wipe test*: The source is wiped with a paper filter, moistened with water; the removed activity is measured.

(3) *Fast immersion in liquid nitrogen*: The source is repeatedly immersed (5 times) in a liquid nitrogen bath at 77 K, for 3 min each time; the removed activity is measured.

(4) *Long Immersion test in liquid nitrogen*: The source is immersed in a liquid nitrogen bath at 77 K for 1 h; the removed activity is measured.

The methods are described in detail in the ENEA internal note [7]. The tests were applied to commercial sources (AEA Technology) and to the sources produced by SORAD. The source intensity varied between ≈ 300 and $\approx 3000\,Bq$. The long immersion (1 h) liquid nitrogen test at 77 K did not show any source leakage at a minimum detectable activity level of approx. 0.01 Bq corresponding to the minimum detectable leakage factor of 8×10^{-6}.

The ^{241}Am WPS were produced for use in three detectors, according to different specifications: a 120 cm wire with 5×12.4 cm-spaced sources for the MEG final Calorimeter (15 wires), a 60 cm wire with 2×12.4 cm-spaced sources for the Calorimeter Prototype (10 wires), a 50 cm wire with a single source for a cryogenic facility at INFN-Pisa (2 wires). Additional 25 disk sources (5 mm in diameter) were also requested. The Am dots were mounted on a gold-plated steel or tungsten wire of diameter $\approx 100\,\mu m$ (Figs. 1 and 2). The resulting wire diameter, after the source mounting, was $< 150\,\mu m$. The dot sources were covered by a protective gold layer $\approx 1.5\,\mu m$ thick. The activity of each Am dot is about 200 Bq with a tolerance

[1] SORAD was recently acquired by Isotope Products Cesio s.r.o.

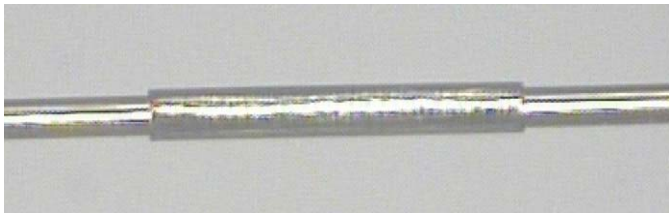

Fig. 1. Micropicture of a Am-source mounted on a 100 μm-diameter wire.

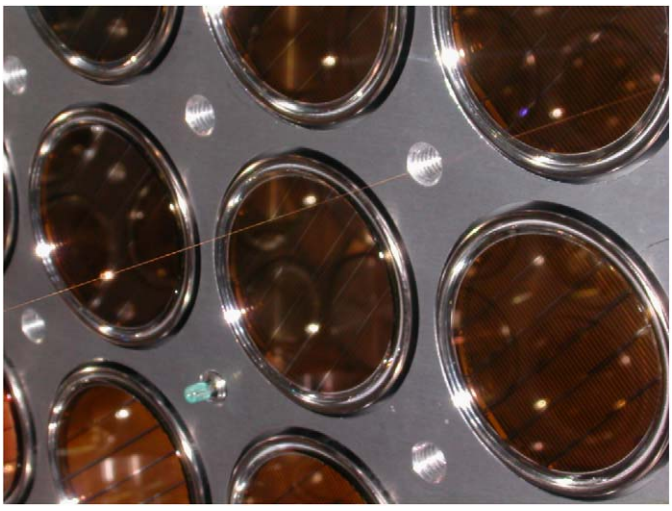

Fig. 2. A two-source wire mounted in the Calorimeter Prototype detector.

±25%. Each dot has a linear dimension $\leqslant 2$ mm. The position of each dot on the wire is precise within 1 mm. A reference mark (non-radioactive !) is mounted on one side of the wire only; the mark (a gold layer fixed by thermocompression) is visible for easy source location.

The 25 *disk-sources* are gold plated disks of diameter 5 mm and have an activity of ≈ 500 Bq per source. Each source is covered by a protective gold layer 1.5 μm thick.

3. Characteristic of the ^{210}Po and ^{241}Am scintillation α-line in gaseous and liquid xenon

The luminescence emitted by rare gases excited by vacuum ultraviolet radiation or particles has been rather well studied for gas, condensed and solid phases [8–14]. A remarkable feature is the close similarity between the emission of gaseous and condensed noble gases. Such a behaviour is due to the fact that in both cases the last relaxation step before the radiative decay is the formation of an excimer, that is a bound state or molecule which exists only in excited electronic state, the fundamental level being a repulsive ground state.

It is also well known that the decay occurs from the two different $^1\Sigma_u^+$ and $^3\Sigma_u^+$ to the $^1\Sigma_g^+$ repulsive ground state giving rise to the "fast" and the "slow" components of the excimer emission, whose spectra practically coincide in width and wavelength [14]. The scintillation mechanism, which involves excited atoms Xe^* and Xe^+ produced by ionizing radiation, can be summarized as follows:

$$Xe^* + Xe \rightarrow Xe_2^* \rightarrow 2Xe + h\nu \tag{1}$$

or

$$\begin{aligned} &Xe^+ + Xe \rightarrow Xe_2^+ \\ &Xe_2^+ + e \rightarrow Xe + Xe^{**} \\ &Xe^{**} \rightarrow Xe^* + \text{heat}, \\ &Xe^* + Xe \rightarrow Xe_2^* \rightarrow 2Xe + h\nu \end{aligned} \tag{2}$$

where $h\nu$ is the ultraviolet photon.

Two things are worth noticing:

(1) The emission of the scintillation photon is either due to excitation or to ionization of Xe atoms, and the two processes exhibit a different time behaviour, as later discussed.
(2) Due to the lack of a bound Xe_2 ground state, the inverse transition $h\nu + Xe_2 \rightarrow Xe_2^*$ is absent. This peculiarity of the excimeric emission is a strong hint for the transparency of noble liquids to self-scintillation light. However, a short attenuation length of scintillation light in liquid xenon has been reported by several authors. Light attenuation is in principle due to absorption and to coherent scattering. There exists clear evidence that, at least in the gaseous phase and in the frequency range about that of scintillation, the attenuation is small and is due to Rayleigh scattering [15].

As apparent from the decay (1) and (2), two different mechanisms contribute to convert energy loss to scintillation light in liquid and gaseous Xe, with different time characteristics. A fast component with two short time constants ($\tau_1 = 4.2$ ns, $\tau_3 = 22$ ns) comes from the de-excitation of singlet and triplet states of excited dimers ($Xe_2^* \rightarrow 2\,Xe + h\nu$). This mechanism is excited mainly by α-sources and fission fragments. Scintillation from relativistic electrons gives, on the other hand, a (comparatively) slow component ($\tau_r = 45$ ns) which is presumably due to the slow recombination between electrons and ions, since this component disappears if some electric field is applied.

The light emission yield for noble gas liquids is usually given in terms of W_{ph}, defined as the average energy needed to produce a scintillation photon. This is related to W_{i}, the average energy to create an electron–ion pair, and to N_{i} and N_{ex}, the number of ionized and excited Xe atoms produced for a deposited energy E_0, by simple relations [9]. The total number of emitted scintillation photons comes from either ionized or excited Xe atoms:

$$N_{\text{ph}} = N_{\text{i}} + N_{\text{ex}} \tag{3}$$

hence the average energy release is

$$W_{\text{ph}} = \frac{E_0}{N_{\text{ph}}} = \frac{E_0}{N_{\text{i}}}\frac{1}{(1 + N_{\text{ex}}/N_{\text{i}})} = W_{\text{i}}\frac{1}{(1 + N_{\text{ex}}/N_{\text{i}})} \tag{4}$$

Table 1
Average energy needed to produce a scintillation photon in liquid Xe for different particles (adapted from Ref. [9])

	W_{ph} (eV)
Relativistic e/γ	23.7 ± 2.4
α-particle	19.6 ± 2.0

where we single out the energy to produce an ion–electron pair $W_i = 15.10\,\text{eV}$.

From Eq. (4), which can be amended including quenching effects and subtracting the contribution of escaping "late" electrons, it is apparent that different ionizing particles could in principle have different N_{ex}/N_i yield due to their different ionization density, hence having different W_{ph}. Values of W_{ph} for electrons, photons and α-particles are reported in the literature, and are summarized in Table 1.

Due to the scintillation mechanism in xenon the self-absorption should be small. Light attenuation is due to (Rayleigh) scattering and absorption processes. The photo-absorption is dominated by impurities in the liquified gas. Two important absorbers are water vapor and molecular oxygen both of which exhibit important absorption lines in the range of interest. Experimentally we proved that, after a suitable purification period, $\lambda_{abs} > 100\,\text{cm}$, at 90% C.L., in LXe [4]. New results with the WPS are presented in Section 7.

4. Reconstruction methods for scintillation events

The light emitted by the WPS travels towards the photomultipliers where it is collected, amplified and recorded by the electronic chain. The information available offline is the charge seen by each PMT, whose 3D position and amplification is precisely known. The amplification is constantly measured and monitored using a series of blue LEDs immersed in the liquid, flashed at different amplitudes, a method that has been shown [4] to give a knowledge of the PMT gains within 3%.

The charge information is used to compute the total number of photoelectrons seen by the calorimeter (Q_{sum}) together with the estimated position of the point-like event, which we will call "full-average":

$$x_{ave} = \frac{\sum_{i\in\{PMT\}} x_i Q_i}{\sum_{i\in\{PMT\}} Q_i} \tag{5}$$

$$y_{ave}, z_{ave} = \text{analogous}. \tag{6}$$

We also compute the weighted average for each calorimeter surface and a MINUIT best-fit of the emission position. This last best-fit is computed by a χ^2-minimization procedure between the observed light distribution on the PMTs and that predicted by taking into account the solid angles corresponding to the PMT photocathodes, as seen from the point of light emission.

For energy measurements, the γ-ray energy is written, in a linear approximation, as a weighted sum of the charges Q_i seen by each PMT:

$$E_l = c + \sum_i c_i Q_i. \tag{7}$$

The coefficients c_i and the constant c can be determined by the so-called "principal component analysis" method [16]. In this method a sample of N ($\sim 10^4$) Monte Carlo events is used to compare the linearized value of the energy, E_l, with the true deposited energy, E_t. A χ^2 expression can be formed:

$$\chi^2 = \sum_{\text{MC events}}^{N} (E_l - E_t)^2 \tag{8}$$

and the coefficients are obtained by the χ^2 minimization. The minimization procedure is analytical and yields the following results:

$$c = \langle E_t \rangle - \left\langle \sum_j c_j Q_j \right\rangle \tag{9}$$

$$c_i = \frac{\mathcal{M}^{-1}}{N-1}\left[\sum_{\text{MC events}}^{N} E_t Q_i - \frac{1}{N}\sum_{\text{MC events}}^{N} E_t \sum_{\text{MC events}}^{N} Q_i\right] \tag{10}$$

where the averages are calculated over the event sample and $\mathcal{M}$ is the covariance matrix (also computed by using the Monte Carlo events):

$$\mathcal{M}_{kl} \simeq \langle (Q_k - \langle Q_k \rangle)(Q_l - \langle Q_l \rangle) \rangle. \tag{11}$$

The unique possibility offered by the liquid scintillation calorimeter, i.e., to have radioactive calibration sources in the bulk of the detector, is affected by the short range of α-particles in liquid xenon (40 μm) comparable to the supporting wire diameter. The short α-range causes part of the emitted light to be intercepted by the wire itself, therefore not reaching the sensitive surface of the PMTs.

The result of this shadowing effect is the appearance, in the reconstructed position plot, of ring structures, as can be seen in Fig. 3. The ring structure can be explained in the following way. Each α-source can be assimilated to a small cylinder with axis along the wire. Photomultipliers surround the cylinder at a certain distance. Due to short α-particle range, each particle emits light only very close to the wire. The light which is not shadowed by the wire reaches the PMTs on the unhindered side. Some weaker light also reaches the PMTs on the opposite side, because part of the light emitted towards the PMTs on the unhindered side is Rayleigh scattered back and, this time, is no longer totally shadowed by the wire. For each coordinate the light source position determination is based on the amount of light reaching opposite side PMTs. If the two amounts are equal, the light source is reconstructed at equal distances from the PMTs, if the two amounts are different, the light source is reconstructed at a position closer to the PMTs more heavily invested by light. The ring structure comes from the fact that the α-particles are equally emitted from the surface of the source cylinder and from the isotropy of the scintillation light. These structures are well reproduced by our Monte Carlo simulation. The

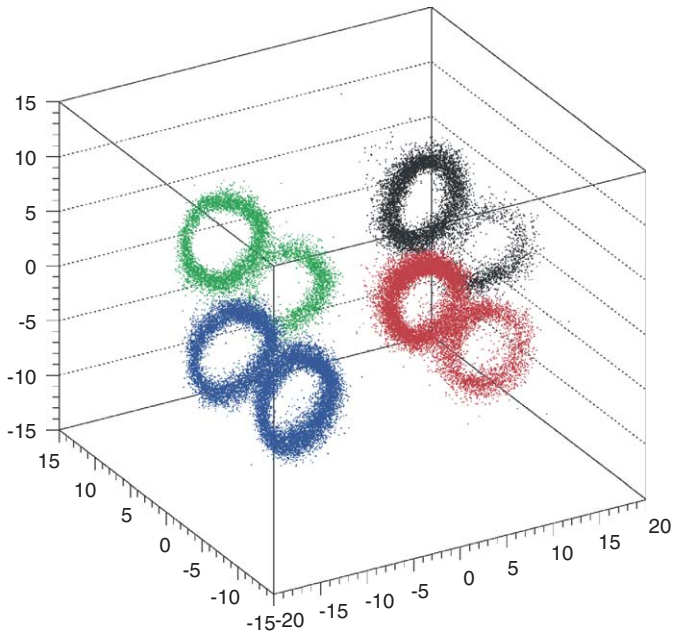

Fig. 3. The 8 rings generated by the α-sources in liquid Xe.

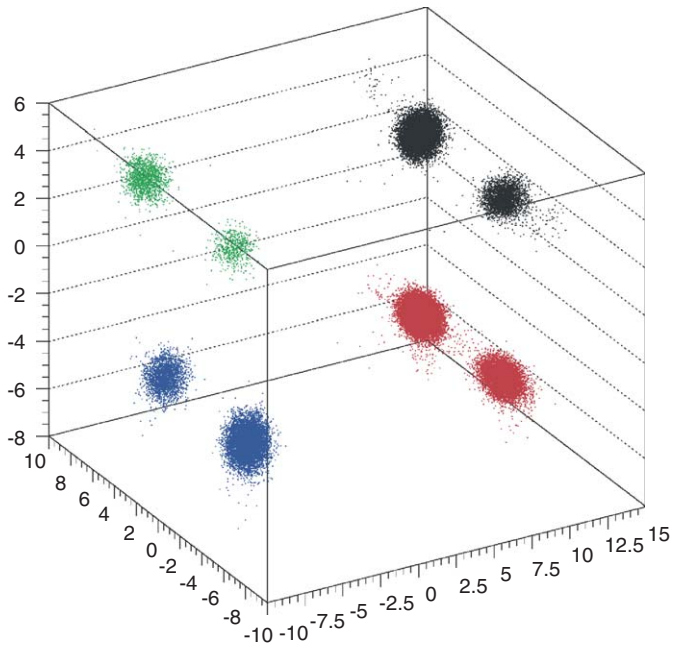

Fig. 4. The 8 blobs generated by the α-sources in gaseous Xe.

size of the ring corresponds to a complex phenomenology and depends on many parameters: the Rayleigh scattering length, the LXe refractive index, the reflectivity of the calorimeter aluminum walls, the reflection and refraction of the PMT quartz windows, the light absorption in quartz, the PMT photocathode reflectivity, etc. While it is possible to obtain a satisfactory agreement between the experimental rings and a Monte Carlo simulation, a real measurement of the various parameters is, at present, quite difficult and it requires further studies. A hope for the future is to obtain a precise measurement of the Rayleigh scattering length in LXe directly coming from a measurement of the ring diameter.

In the gaseous phase, on the other hand, being the α-range much larger than the typical wire dimension (range ~7 mm), the shadowing effect is negligible and the position of the α-sources on the wires is reconstructed as a 3D Gaussian of 3 mm $\sigma_{x,y,z}$ centered at the nominal source position (see Fig. 4). The close similarity between the light emission in the gaseous and the liquid phases is therefore essential, since we can use the gas data, in which the rings are not present, to compute QEs. Furthermore, in gaseous Xe the absorption length and the Rayleigh scattering length are very large and the refractive index $n_{\mathrm{GXe}} = 1$.

5. Determination of the PMT QEs and amplifications

The relative QEs of all PMTs are extracted, in gaseous Xe, from the comparison of the pulse charge with the charge expected from our Monte Carlo simulation. To minimize temperature-dependent effects, the QE runs were taken at low temperature (203 K), as close as practically possible to that of LXe (163 K).

The reason of using gaseous Xe is, as already noted, twofold: the α-sources are perceived as point-like (i.e. no wire shadow effect) and in the gaseous phase absorption and scattering of the Xe scintillation photons can be neglected. The similarity of the emission spectra in the two phases is expected to give QEs in gas which should coincide with the ones in liquid (see later). We will show that the application of the obtained QEs improves very much the energy and position reconstruction of (photon) events inside the detector. The QE is evaluated as follows: for each photo-multiplier we compute the expected number of photoelectrons due to each α-source via a Monte Carlo simulation, assuming infinite Rayleigh scattering and absorption lengths, the refractive index for Xe $n_{\mathrm{GXe}} = 1$ and equal QEs for all PMTs. We extract the corresponding experimental quantities by fitting the α-data in gas. Since the average number of photoelectrons expected at each PMT is very low (sometimes less than one) we fit the data by using a Poisson function (see Fig. 5). Data points are plotted versus Monte Carlo predictions: the expected linear relation is well verified (see Fig. 6) for a large number of PMTs. The slope of the fitted straight line represents our QE estimate. The distribution of the measured quantum efficiencies is shown in Fig. 7. To get a better evaluation of the QEs, several runs of α-sources in cold gas were used. We estimate that this procedure gives the QEs at a 10% level. The average uncertainty, on the other hand, can be estimated by comparing, PMT by PMT, the quantum efficiencies extracted with the above method in different runs, separated by a long time period (months) in which the calorimeter was evacuated, re-filled and the α-source positions were changed. The PMT QEs were also measured in liquid Xenon. In this case, a full simulation based on the LXe optical properties is needed to extract the QEs from

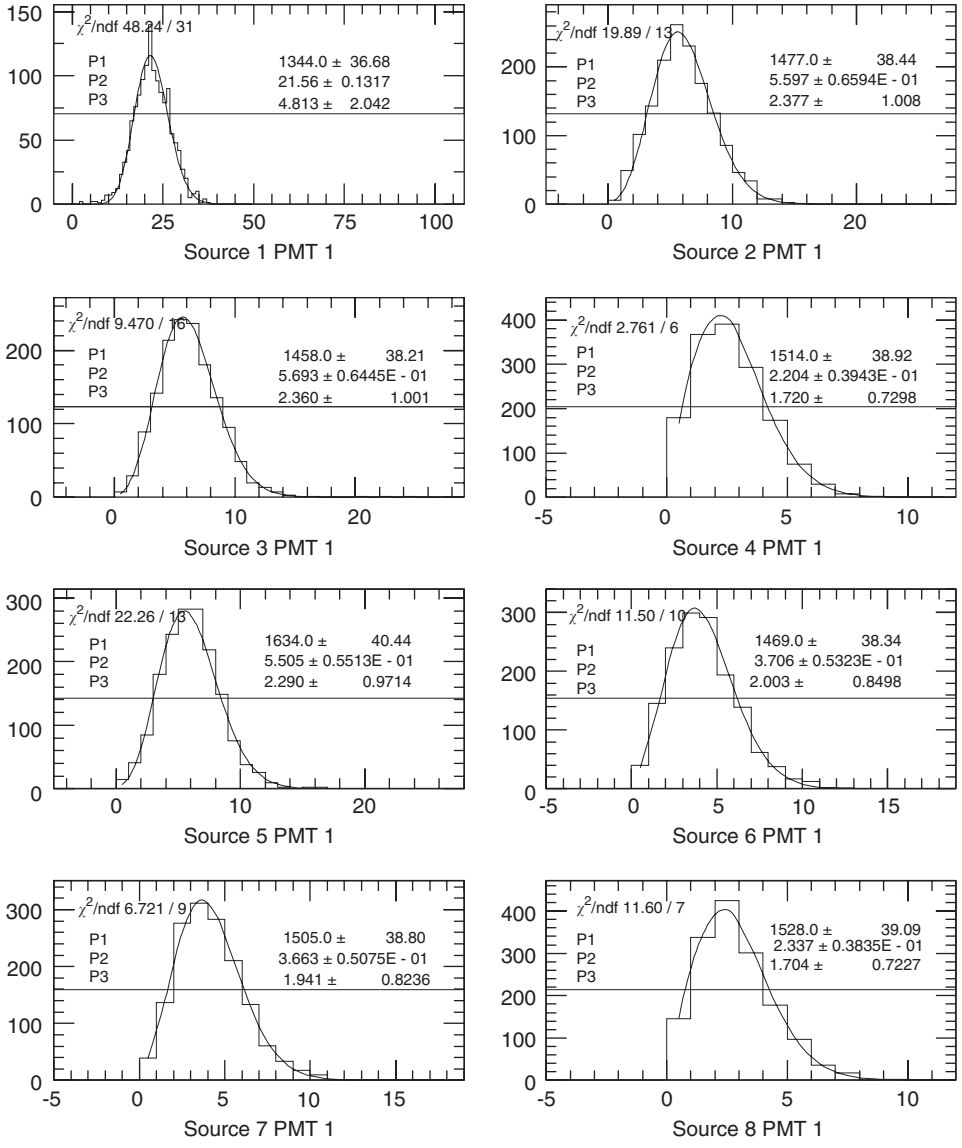

Fig. 5. Examples of Poisson fits to the PMT charge distributions.

the data collected with the Calorimeter Prototype. The correlation between the PMT QEs, measured in gas and in liquid, is rather good, as it appears in Fig. 8. We point out that only relative QEs are measured in both cases.

The Calorimeter Prototype was used, after the determination of all PMT QEs, to measure γ's from π^0 decays from π^--capture on hydrogen, at rest. One of the two γ's was detected in the Calorimeter Prototype, the second γ was detected by a large NaI which was also ensuring the two γ collinearity (54.9 and 82.9 MeV γ's entering the Calorimeter Prototype). We show in Fig. 9 the improvement in the width of two γ-lines due to the QE optimization.

6. Pulse shape discrimination in LXe

We already discussed in Section 3 the modes of light emission in LXe and their dependence on the ionization density. α-particles are associated with shorter light emission times, while muons, electrons and photons are associated with longer times. This is clearly seen in Fig. 10 where the recorded pulses corresponding to an α-particle and to a cosmic-ray μ are normalized in pulse-height and compared. A particle pulse-shape discrimination is therefore possible in LXe. We have demonstrated this by an acquisition run with the Calorimeter Prototype (containing several α-sources) exposed close to the high intensity μ-beam of the MEG experiment, the MEG beam generating an electromagnetic background in the calorimeter at a much higher level of intensity than the one of the α-sources. The recorded events, corresponding to the sum of 32 PMT waveforms, were classified according to the simple variable Q/A, where Q indicates the integral of the sum pulse-shape and A the maximum pulse-amplitude. The Q vs. A plot of all events is shown in Fig. 11. There is the obvious Q, A correlation, and the α-particles are clearly separated from the events of electromagnetic origin. A bi-dimensional plot

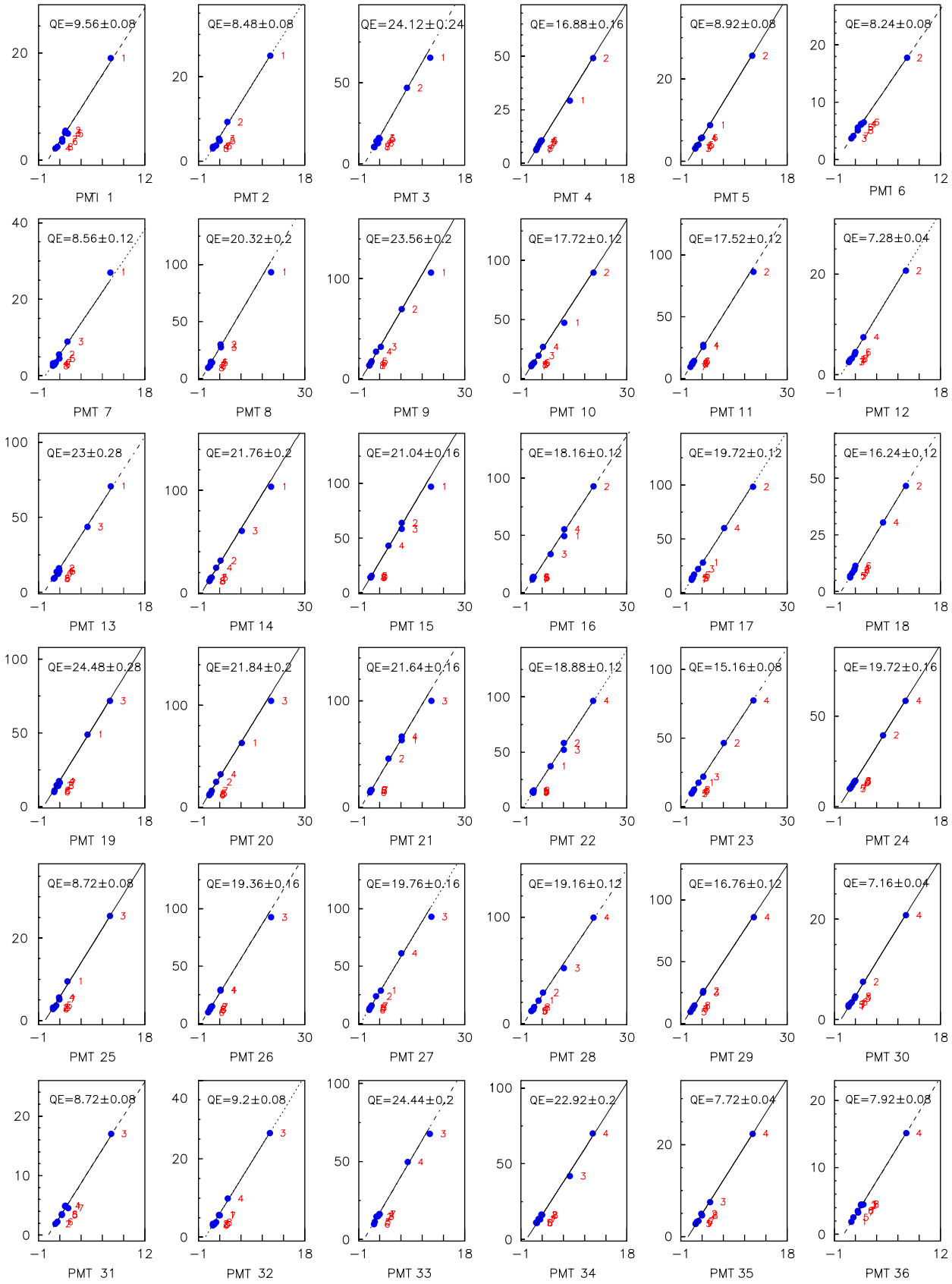

Fig. 6. Examples of linear fits to extract the PMTs quantum efficiencies. QE fits for 36 different PMTs, each looking at eight α-sources. Measured vs. expected number of photoelectrons.

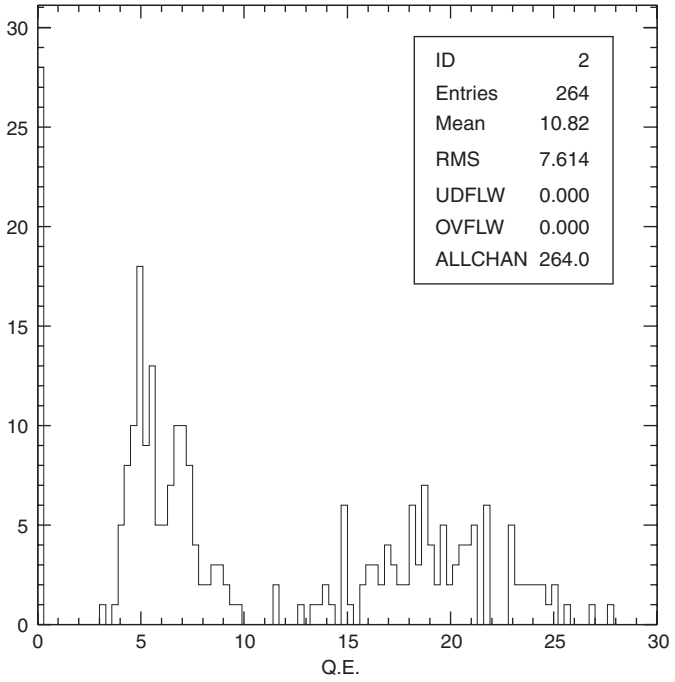

Fig. 7. The distribution of the measured quantum efficiencies for all the PMTs. The two clusters in the QE distribution correspond to two different photocathode types.

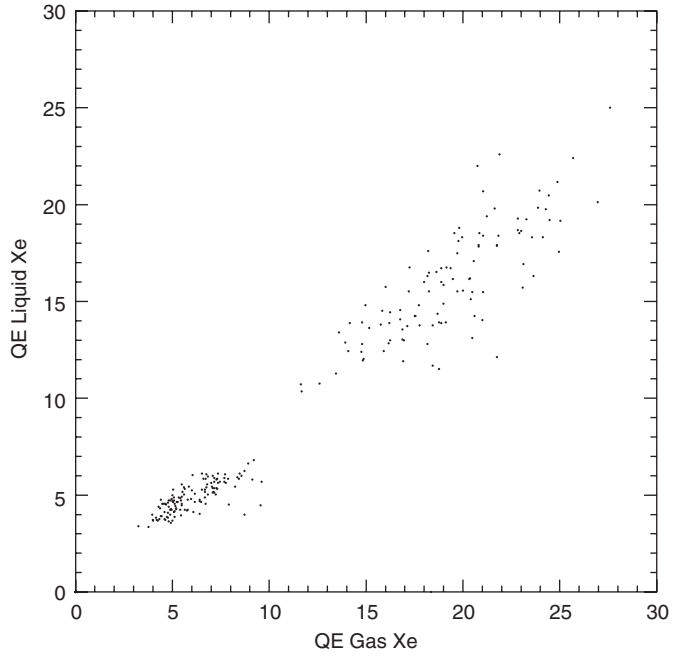

Fig. 8. Comparison of the PMT QEs measured in gas Xenon and in liquid Xenon. The correlation between the two determinations is rather good. (We only measured relative QEs.)

of the x- and y-coordinates of all events is shown in Fig. 12. If one selects the events (red) classified as α-particles in the previous plot, one can observe that the events originate at the known positions of the α-sources. The pulse-shape discrimination method, we just described, can be directly

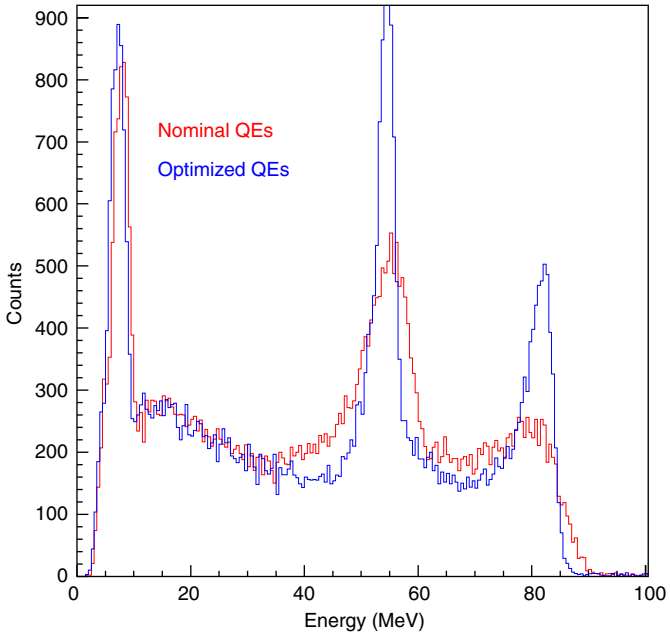

Fig. 9. 54.9 and 82.9 MeV γ-lines before and after the PMT QE optimization.

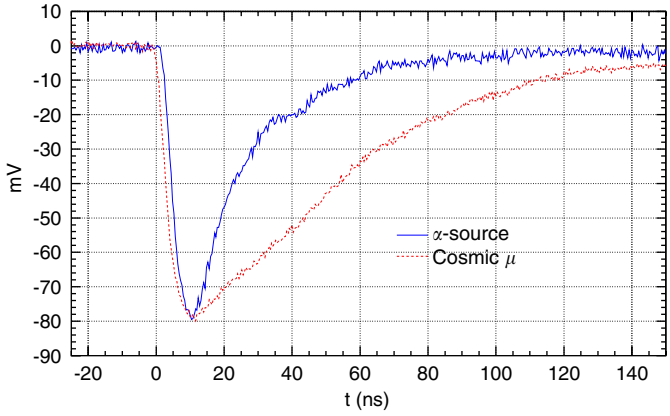

Fig. 10. Pulse shapes due to an α-particle (continuous-line) and to a cosmic-ray μ (dotted-line), as recorded by a digital oscilloscope of bandwidth 300 MHz and sampling frequency 2.5 GHz.

implemented in the MEG trigger system and it will be used to select the calibration events generated by the α-sources.

7. Absorption length estimate

If one introduces the quantities $\lambda_{\rm att}, \lambda_{\rm abs}, \lambda_{\rm diff}$, where $\lambda_{\rm att}$ enters the expression for the light attenuation in LXe, one obtains $I(x) = I_0 e^{-x/\lambda_{\rm att}}$ and the three characteristic lengths are related by

$$\frac{1}{\lambda_{\rm att}} = \frac{1}{\lambda_{\rm abs}} + \frac{1}{\lambda_{\rm diff}}. \quad (12)$$

$\lambda_{\rm abs}$ corresponds to a real absorption of photons, which are then lost for good. $\lambda_{\rm diff}$ is related to photon elastic scattering and it can be assumed to coincide with $\lambda_{\rm R}$, the Rayleigh scattering length. We discussed the LXe optical

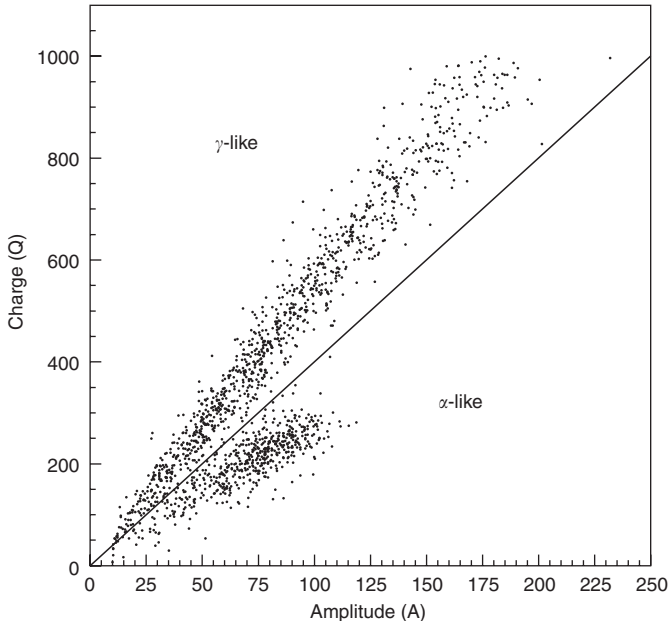

Fig. 11. Distribution of Q vs. A (i.e.: pulse-charge vs. pulse-amplitude) for all events generated by α-particles and by the e.m. background due to the normal MEG μ-beam.

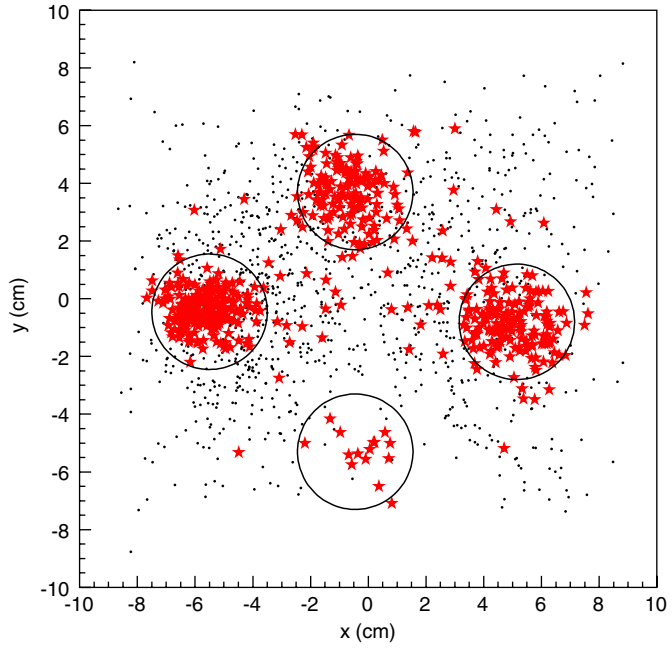

Fig. 12. xy positions of all events. The red points correspond to events having $Q/A \leqslant 4$. Those events cluster at the known positions of the α-sources.

properties in Ref. [4], where we explained the procedure for measuring λ_{abs} and gave the first experimental upper limit for that quantity. The measurement was recently improved by the use of the WPS and a better determination of the PMT QEs. We present in Fig. 13 a comparison between the light yield data in LXe and the corresponding Monte Carlo simulation, as a function of the distances between the

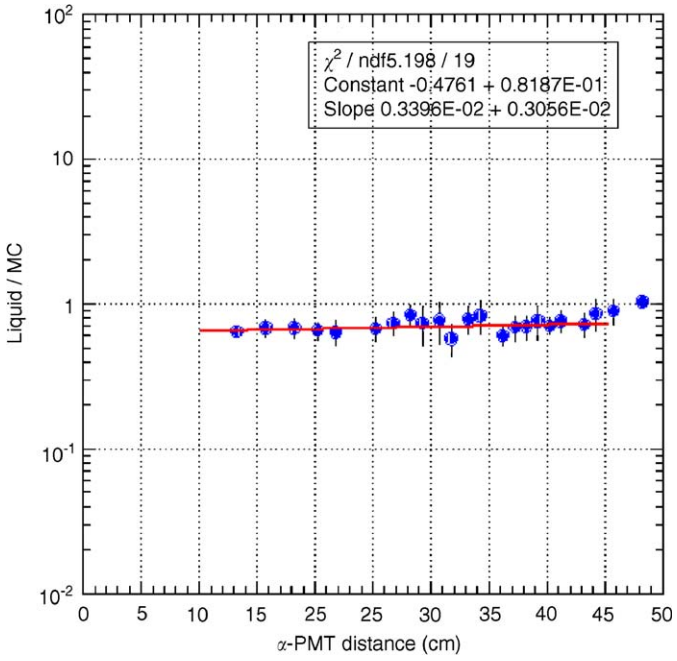

Fig. 13. Comparison of light yield data and Monte Carlo simulation, as a function of the distances between α-sources and PMTs. The resulting absorption length is $\lambda_{abs} > 3$ m at 90% C.L. (see text).

α-sources and the PMTs. The resulting absorption length is $\lambda_{abs} > 3$ m at 90% C.L. The improvement over the previous result is mainly due to smaller systematic errors.

8. Conclusions

A calibration technique based on a radioactive ^{241}Am point-source lattice was developed and applied, for the first time, in a prototype of the MEG liquid xenon calorimeter. The method is particularly valuable for liquid detectors (cryogenic noble gas or liquid scintillator detectors) in which the radioactive sources can be positioned within the scintillating material. It allowed the determination of the PMT QEs and the determination of a lower limit for the LXe λ_{abs} in the UV.

References

[1] The MEG experiment: search for the μ → eγ decay at PSI. Proposal to PSI, Proposal to INFN at ⟨http://meg.web.psi.ch/docs/index.html⟩.
[2] MEGA Collaboration, M. Ahmed, et al., Phys. Rev. D 65 (2002) 112002.
[3] R. Barbieri, L.J. Hall, Phys. Lett. B 338 (1994) 212;
R. Barbieri, L.J. Hall, A. Strumia, Nucl. Phys. B 445 (1995) 219.
[4] A. Baldini, et al., Nucl. Instr. and Meth. A 545 (2005) 753 and references therein.
[5] A. Baldini, et al., MEG Internal note TN027, Considerations on the Calibration and monitoring of the MEG detector, May 02, 2005.
[6] ⟨http://www.raz-dva.cz/sorad/⟩.
[7] P. De Felice, et al., Leakage tests for Am-241 solid sources used for liquid xenon detector monitoring. ENEA Internal Note and Nucl. Instr. and Meth. A 560 (2006) 640.

[8] T. Doke, Port. Phys. 12 (1981) 9 in: T. Ferbel (Ed.), Experimental Techniques in High Energy Physics, Addison Wesley, 1987.
[9] T. Doke, K. Masuda, Nucl. Instr. and Meth. A 420 (1999) 62.
[10] R. Bernabei, et al., Nucl. Instr. and Meth. A 482 (2002) 729.
[11] A.S. Schlüsser, et al., Appl. Phys. Lett. 77 (1) (2000).
[12] E. Morikawa, et al., J. Chem. Phys. 91 (1989) 1469.
[13] J. Jortner, et al., J. Chem. Phys. 42 (1965) 4250.
[14] N. Schwenter, E.E. Koch, J. Jortner, "Electronic Excitations in Condensed Rare Gases", Springer, Berlin, 1985.
[15] J.D. Jackson, Classical Electrodynamics, Wiley, New York.
[16] S. Belforte, et al., SVT Technical Design Report, 807-CDF note 3108, 1994; CERN-EP report 81-12/Rev.